Chapter

Electronic Transport in Few-Layer Black Phosphorus

Gen Long, Xiaolong Chen, Shuigang Xu and Ning Wang

Abstract

Subjected to an adequately high magnetic field, Landau levels (LLs) form to alter the electronic transport behavior of a semiconductor. Especially in two-dimensional (2D) limit, quantum Hall effect sheds light on a variety of intrinsic properties of 2D electronic systems. With the raising quality of field effect transistors (FET) based on few-layer black phosphorus (BP), electronic transport in quantum limit (quantum transport) has been extensively studied in literatures. This chapter investigates the electronic transport in few-layer BP, especially in quantum limit. At the beginning of this chapter, a brief introduction to the background of LL, edge state, and quantum Hall effect will be delivered. We then examine the fabrication of high-quality FET based on BP and their electronic performances followed by exploring the magnetoresistances of these high-quality devices which reveal Shubnikov-de Haas (SdH) oscillations and quantum Hall effect in BP. Intrinsic parameters like effective mass, Landé g-factor, and so on are discussed based on quantum transport.

Keywords: black phosphorus, field effect transistor, mobility, Landau level, quantum hall effect

1. Introduction

Developing high-quality functional materials such as high-mobility semiconductors is an essential process to explore fundamental condensed matter research. The recent rediscovery of BP as a new member of 2D materials with theoretically predicted high mobility and widely tunable electronic bandgap makes it promising for various electronic devices and for probing interesting physical phenomena [1–4]. However, there are various obstacles to overcome in order to achieve the theoretically high carrier mobility in few-layer BP. Those obstacles include degradation of flake quality in atmosphere environment, electronic scatterings (against charge impurities, crystal defeats, and so on), high contact resistance, and so on. In devices without high enough mobility, new physical phenomena can be smeared out due to a large charge carrier scattering rate.

Since Landau level (LL) is crucial to understanding the physical phenomena in quantum transport process, we would like to deliver a brief idea about it here. For clarity, we will neglect the spin degeneracy at first and will come to it when necessary. Consider an electronic system without electronic interactions in an applied magnetic field along z direction and the magnetic field strength is B:

$$\boldsymbol{B} = \begin{pmatrix} 0 \\ 0 \\ B \end{pmatrix} \tag{1}$$

In Landau gauge (the wave function is gauge invariant),

$$\boldsymbol{B} = \nabla \times \boldsymbol{A} = \nabla \times \begin{pmatrix} 0 \\ Bx \\ 0 \end{pmatrix} \tag{2}$$

where $\boldsymbol{A}$ is the electromagnetic vector potential. The Hamiltonian of this system is then

$$H = \frac{1}{2m}(\boldsymbol{P} - e\boldsymbol{A})^2 = \frac{p_x^2}{2m} + \frac{1}{2m}\left(p_y - eBx\right) \tag{3}$$

where e stands for electron charge, $\boldsymbol{P}$ is the canonical momentum, and m is the mass of charge carriers. Solving this Hamiltonian we get,

$$\begin{aligned} E_n &= \hbar\omega(n + 1/2) \\ \boldsymbol{\omega} &= \frac{e\boldsymbol{B}}{m} \end{aligned} \tag{4}$$

where ω is the cyclotron frequency and $\hbar$ is the reduced Planck constant. Clearly, the eigen energy of electrons are separated and equally spaced. The energy gap between two adjacent LLs is $\hbar\omega$. Furthermore, by studying the electronic systems in finite regime, the degeneracy (g_L) of LL per unit area is derived to be,

$$g_L = \frac{eB}{2\pi\hbar} \tag{5}$$

Now we take the spin of electron into consideration. Besides the formation of LLs, the energy of electron is also split by Zeeman effect $E_Z = g\mu_B B$, where $\mu_B = e\hbar/2m_0$ (m_0 is free electron mass) is the Bohr magneton and g is the Landé g-factor. Interestingly, the Zeeman splitting coincides precisely with the energy gap between LLs $E_C = \hbar\omega = e\hbar B/m$ [5], for free electrons ($g = 2, m = m_0$). It means that spin-up electrons in n_{th} LL exhibit the same energy with spin down ones in $(n+1)_{th}$ LLs. However, this coincidence usually does not happen in real material systems because of the deviations of effective mass from m_0 and g-factor from 2. Nevertheless, this coincidence can be realized by tilting the magnetic field to adjust the ratio between E_C and E_Z which would be discussed hereafter.

We conclude now that under applied magnetic field, electrons cycle in quantized traces with quantized energy in one direction. However, when these traces intersect the edge of the electron system, these electrons cannot complete the full cyclotron. Instead, they bounce back and enter another adjacent traces because the cycling direction is fixed. As a result, electrons near the edge are in a skipping motion along one-dimensional boundary moving in a single direction, which is referred to as chiral edge states. Due to the absence of scattering, the edge states carry electronic current with no voltage drop, i.e., $R_{xx} = V_{xx}/I_{channel} = 0$. Electrons near different edges move in different directions to ensure that the net current, in the absence of electric field, is zero.

When an in-plane electric field is applied, electrons are accelerated along one direction. As a result, the balance between the occupation of edge states in two

opposite sides is broken, i.e., more electrons are filled in the edge states in one boundary. As we have discussed before, the energy of electrons is quantized. Consequently, the Hall conductance $\sigma_H = \frac{I_{channel}}{V_H}$ is quantized. Analysis into more details leads to $\sigma_H = \nu \frac{e^2}{h}$, where $\nu = 1, 2, 3...$ is integer.

Alternatively, quantum Hall effect can be understood based on Berry phase [6]. Consider an adiabatic system in which the eigenstate evolves with external parameters slowly. When the external parameters make up a loop and come back to itself, the eigenstate should also come back to itself (let us rule out the possibility of degeneracy here) but with a different phase, because the eigen energy of eigenstates with different phases is invariant. This phase is the so-called Berry phase. This Berry phase manifests itself in an electronic system through weak localization effect, A-B effect, and so on. All these effects come from the dynamics of electrons. For Bloch electron under the perturbation of a weak electric field $\boldsymbol{E}$, its velocity $\boldsymbol{v}$ with a given wave vector $\boldsymbol{k}$ becomes

$$\boldsymbol{v}(\boldsymbol{k}) = \frac{\partial \varepsilon(\boldsymbol{k})}{\hbar \partial \boldsymbol{k}} - \frac{e}{\hbar} \boldsymbol{E} \times \boldsymbol{\Omega}(\boldsymbol{k}) \tag{6}$$

where ε is the energy of electron and $\boldsymbol{\Omega}$ is the Berry curvature. The first term is the result of band dispersion. The second term which is absent in classic Bloch theorem is more interesting. It describes a velocity perpendicular to the applied electric field which will give rise to the Hall effect without magnetic field. With this transverse contribution to velocity, the Hall conductivity is given by

$$\sigma_{xy} = \frac{e^2}{\hbar} \int_{BZ} \frac{d^2k}{(2\pi)^2} \Omega_{k_x k_y} \tag{7}$$

where the integration is over the entire Brillouin zone and the result of this integration is the Chern number ν of the Brillouin zone ($\nu = 0$ when external magnetic field is zero). Therefore, the Hall conductivity is

$$\sigma_{xy} = \nu \frac{e^2}{h} \tag{8}$$

This reaches the same conclusion with previous analysis, i.e., the Hall conductivity is quantized.

In this chapter, we would introduce the detailed work on BP from the characterization of the electronic transport process and figure out the main limitation to high-quality devices, followed by efforts to conquer the impediment. Once devices with high enough quality can be fabricated, we will go to the electronic transport in quantum limit (cryogenic temperature and high magnetic field). Realization of quantum transport process in BP allows people to determine some critical parameters (effective mass, Landé g-factor, and so on) which are crucial for seeking engineering applications of this material.

2. High-quality FET based on BP

In 2014, several groups first demonstrated the FET based on few-layer BP (**Figure 1a**) [1, 3, 7, 8], giving rise to the renaissance of BP. As a semiconducting layered material, BP has a high carrier mobility at room temperature, with the value up to 1000 $cm^2V^{-1}s^{-1}$ at the first demonstration of its FET, owing to its relatively

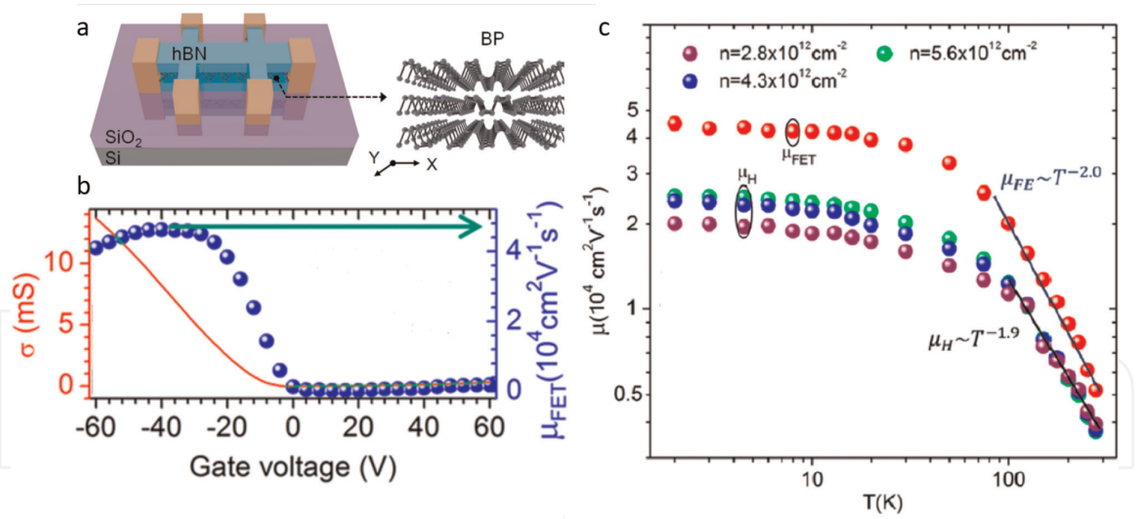

Figure 1.
High-mobility BP FET. (a) Schematic of FET device based on encapsulated BP. The right panel shows the crystal structure of BP. (b) Transfer curves of high-mobility BP devices at cryogenic temperature accompanied with the corresponding FET mobility. (c) Temperature dependence of FET mobility and hall mobility. Panel (a) is reproduced with permission from NPG [12]. Panels (b) and (c) are reproduced with permission from ACS [10].

weak electron-phonon interaction [3]. Meanwhile, the FET's current on-off ratio exceeds 10^5, which indicates the promising electronic application of BP-based devices [2, 3, 9]. Up to now, the record room temperature hole mobility achieved in experiments arrives 5200 $cm^2V^{-1}s^{-1}$, almost approaching the theoretical phonon scattering limitation ranging between 4800 and 6400 $cm^2V^{-1}s^{-1}$ for few-layer BP [10]. The high mobility and desirable current saturation of BP at room temperature offer advantages for high-frequency electronic and optoelectronic applications [11]. At cryogenic temperatures, the FET hole mobility can be even up to 45,000 $cm^2V^{-1}s^{-1}$ as shown in **Figure 1b** and **c** [10], the highest value among the presently reported 2D semiconductors. The ultrahigh mobility in BP at low temperature makes it as a unique platform for studying the quantum transport in 2D semiconductors.

As the most famous elemental layered material beyond graphene, BP provides the needed bandgap for FET applications, especially in infrared region. Unlike semiconducting transition metal dichalcogenides (TMDCs), the bandgap in BP is direct for all number of layers, which makes this material particularly promising for optoelectronic applications. Moreover, the bandgap of BP is widely tunable achieved by layer number, electric field, strain, and alloying. Combined with its strong anisotropic, BP may allow for the exploration of new exotic phenomena and multifunction devices.

2.1 Realization of air-stable devices based on BP

Although bulk BP is considered as the most stable allotrope of phosphorus, it is reported that few-layer BP is unstable in ambient conditions. Significant surface roughening over the time after exfoliation can be observed by AFM [8]. The investigation of water condensation on BP flakes reveals that BP is very hygroscopic and tends to uptake moisture from air [13]. Long-time exposure to air can even etch BP away. The in situ Raman and transmission electron spectroscopy studies of the degradation of BP show that the degradation in air mainly arises from the photo-assisted oxidation reaction with oxygen dissolved in the adsorbed water on its surface [14]. Theoretical work revealed that BP presents a strong dipolar moment out of plane which makes it very hydrophilic [15].

The environmental instability of BP flakes makes it a challenge to fabricate high performance BP-based devices, since most experiments reported on BP relied on mechanically exfoliated flakes. To prevent the degradation, several kinds of passivation were developed. Atomic layer-deposited AlO_x overlayers effectively suppress ambient degradation, preserving the intrinsic high carrier mobility and on-off ratios in BP FETs [16]. Alternatively, encapsulating BP by a polymer superstrate, such as PMMA, can also suppress the oxidation [8, 17]. Moreover, it was demonstrated that hexagonal boron nitride (*h*BN) can be effectively used for passivation of BP [9, 18–21]. The devices fabricated by *h*BN-encapsulated BP showed air-stable performance and hysteresis-free transport characteristics in ambient conditions, without observable decrease in carrier mobility or on-off ratio after few weeks' exposure in air [9, 18]. Furthermore, *h*BN is an insulating layered material, providing atomically thin clean surface and dielectric environment. Before the rediscovery of BP, it was already reported that *h*BN can significantly improve the mobility of graphene-based devices [22, 23]. Researchers found that by applying the *h*BN encapsulation technique in graphene to BP (**Figure 2**), the mobility of BP-based FETs can increase to several 1000 $cm^2V^{-1}s^{-1}$ [9, 24], later even up to 45,000 $cm^2V^{-1}s^{-1}$ [10] at cryogenic temperatures.

2.2 Ohmic contact and ambipolar transport in BP

As that in other semiconducting devices, the electrical performance of devices based on BP is significantly affected by the electrical contacts. Low contact resistance is critical to achieving high mobility, high on-off ratio, and large photo response in BP. The main issue in BP-based FET is the existence of large Schottky barrier in the contacts, which limits the current injection and its potential for applications. Several kinds of contact engineering have been identified toward high-quality electrical contacts. By choosing various metals with different work functions to match BP, different performance of BP transistors can be achieved [26, 27]. The aluminum-contacted BP displays ambipolar characteristic with nearly symmetric electron and hole mobility of 950 $cm^2V^{-1}s^{-1}$ in 13 nm flake and unipolar *n*-type

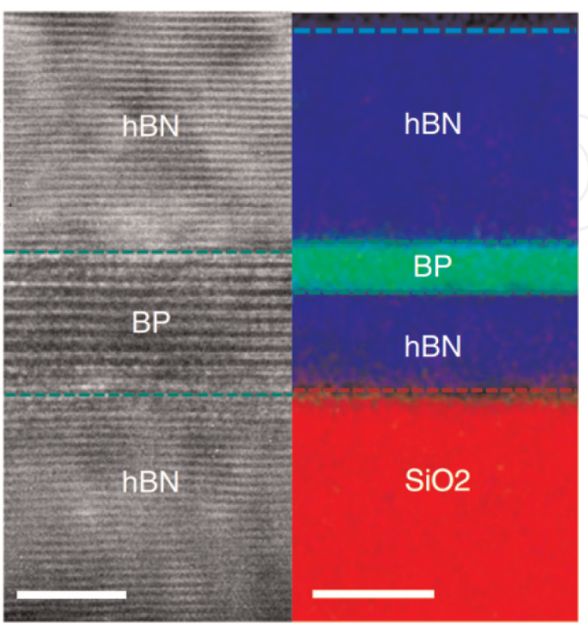

Figure 2.
The cross-section HR-TEM image of the hBN/BP/hBN *structure. The right panel shows the element analysis for nitrogen (blue), phosphorus (green), and oxygen (red). Scale bars: 4/10 nm (left/right). This figure is reproduced with permission from NPG [25].*

behavior in 3 nm flake, while the palladium-contacted BP shows p-type dominated transport behaviour in thick flakes. Besides traditional metallic contacts, graphene can also be used as a contact medium to BP. Graphene has an atomically flat surface, and its work function can be tuned by gate voltages, which leads to the elimination of Schottky barrier height using graphene electrodes [18]. In addition, to reduce the contact resistance, monolayer hBN can be inserted between metal films and BP by van der Waals transfer technique [20]. The monolayer hBN acts as a tunnel barrier with relatively high tunnel conductivity. If bilayer hBN is used as the tunnel barrier, it results in a higher contact resistance with a factor of 10 than that in monolayer hBN. In hBN-encapsulated BP devices, selective area etching technique was used to open the window to make the contact [9]. By using appropriate etching recipe, the top hBN can be quickly etched, while BP layer still survives, ensuring the metals directly contact with the plasma-treated BP. Low contact resistance down to several $k\Omega \cdot \mu m$ can be achieved even at low temperature. Surprisingly, this selective area etching technique can be effectively applied to other 2D semiconductor such as TMDCs with high performance [28].

Few-layer BP has a direct bandgap with the size around 0.3 eV. The small bandgap of few-layer BP facilitates the injections of both electron and hole, resulting in ambipolar characteristic being easily observed in BP-based transistors. The ambipolar transport in BP can exploit both n-type and p-type in a single transistor, with the mobility of both electron and hole at a high value of several thousand $cm^2V^{-1}s^{-1}$ [29], which provides the promising applications in complementary metal-oxide semiconductors and 2D material-based memory devices [30]. The possibility of manipulation in a single ambipolar transistor without external doping or ion implantation process simplifies the BP-based nanotechnology in feature's industrial application. The ambipolar functionality and high mobility of BP help the realization of flexible ambipolar inverter, frequency doubler, inverting and noninverting analogy amplifiers, and amplitude-modulated demodulator [31]. Furthermore, the ambipolar operation of BP can be locally controlled by electrostatic gating to form gate-defined PN junction [32]. Under illumination, these PN junctions show strong photocurrent due to photovoltaic effect, attractive for energy harvesting in the near-infrared.

2.3 Strong transport anisotropy in BP

BP has a puckered honeycomb lattice, yielding strong in-plane anisotropy. The unusual anisotropic structure of BP results in its strong in-plane anisotropic electrical and optical properties. BP-based devices with electrode probes fabricated at various angles have been used to probe the electrical conductivity and carrier mobility along different direction (**Figure 3**) [1, 7]. Higher hole mobility and conductivity were found along light effective mass directions (x-direction) [1, 9]. The experimental results verified the theoretical calculations, which predicted that the effective mass in few-layer BP along x and y directions are $m_x \sim 0.14\, m_0$ and $m_y \sim 0.89\, m_0$, respectively [2]. Not only electrical properties but also optical properties of BP show strong in-plane anisotropy, such as optical absorption and polarized Raman spectrum in few-layer BP [1] and photoluminescence in monolayer BP [33].

2.4 Widely tunable electronic bandgap

Due to the strong layer interaction and quantum confinement of the charge carriers in the out-of-plane direction, BP shows stronger thickness-dependent bandgap compared with other 2D semiconductors, such as TMDCs. When the

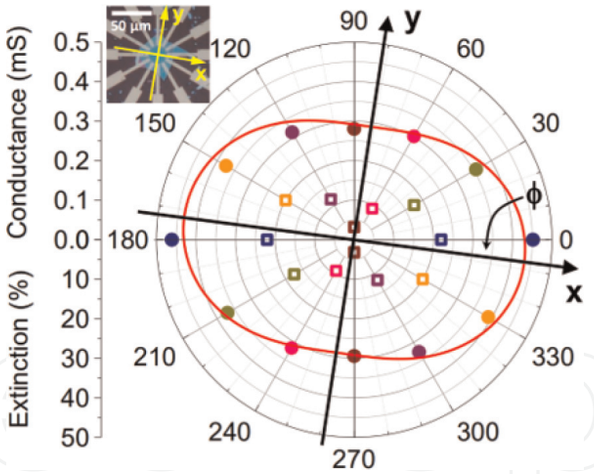

Figure 3.
Anisotropic transport of BP. This figure is reproduced with permission from NPG [1].

thickness of BP decreases from bulk to monolayer, its direct bandgap was predicted to increase roughly from 0.3 to 2.0 eV [34]. This prediction has been experimentally confirmed by the measurements of optical absorption [35]. The optical bandgaps of monolayer, bilayer, trilayer, and bulk BPs were determined to be 1.73, 1.15, 0.83, and 0.35 eV, respectively. The bandgap of few-layer BP is also widely tunable by electric fields. By using an in situ potassium doping technique, a vertical electric field from dopants modulates the bandgap of few-layer BP and even tunes the system to an anisotropic Dirac semimetal state, owing to the giant Stark effect [36]. For practical applications, the dynamic tuning of bandgap can be realized by the dual-gate FET configuration in BP-based devices [37]. For example, the transport measurement in a 10-nm-thick BP flake shows that its bandgap can be continuously tuned from 0.3 eV to below 0.05 eV, using a moderate displacement field of 1.1 Vnm^{-1}. Local-strain engineering was demonstrated to be another way to control the bandgap in BP. When BP is subjected to a periodic strain, remarkable shift of optical absorption edge up to 0.7 eV was detected [38]. When BP-based FETs fabricated flexible substrates, the applied mechanical strain continuously modulates its bandgap, significantly altering the density of thermally activated carriers. As a result, large piezo-resistive effects were observed at room temperature [39]. Another way to tune the bandgap of BP includes alloying. Successful synthesis of layered black arsenic-phosphorus with tunable compositions allows the bandgap of alloyed BP to be changed from 0.3 to 0.15 eV [40], making black arsenic-phosphorus as a promising candidate for long-wavelength infrared photodetectors [41, 42].

3. SdH oscillation and quantum hall effect in BP

Upon subjection to a magnetic field, LLs form in an electronic system. However, high scattering rate of charge carriers leads to a broadening of LLs. The LLs manifest itself only when this broadening is lower than the energy gap between two adjacent LLs. The achievement of high-quality devices (high carrier mobility and low scattering rate) suppresses this broadening and finally allows the observation of LL with laboratory reachable magnetic fields. By the end of 2014, Li et al. and Nathaniel et al. reported the first observation of Shubnikov-de Haas (SdH) oscillations in BP hole system [3, 24] (**Figure 4a**). Later on Li et al. observed the quantum Hall effect in the same system (**Figure 4b**) [43]. **Figure 4a** shows ΔR_{xx} (a smooth background subtracted from R_{xx}) and striking patterns of SdH oscillations,

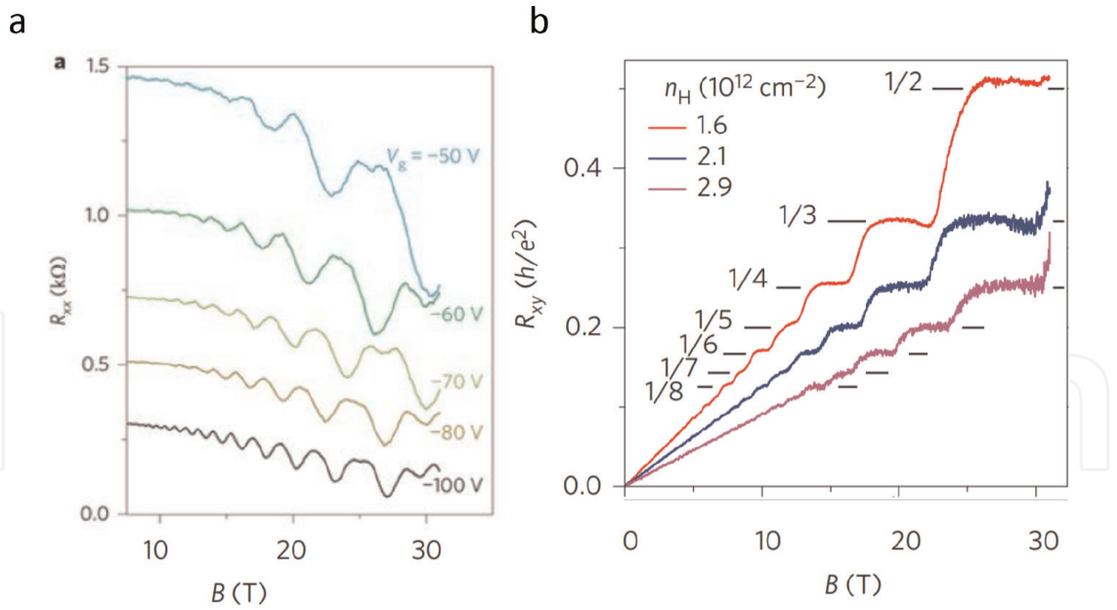

Figure 4.
Quantum transport in BP. (a) R_{xx} versus V_g and magnetic field B. (b) Hall resistance $R_{xy} = V_{xy}/I$ variation with magnetic field at cryogenic temperature. The quantized plateaus demonstrate the quantum Hall effect in BP two-dimensional hole gas. This figure is reproduced with permission from NPG [43, 44].

appearing along straight lines, are clearly resolved. When the Fermi level of the 2D hole system is located at the center of certain LLs (at the middle of two adjacent LLs), the system exhibits high resistance (low resistance). Hence the oscillations are employed as a powerful tool to monitor the evolution of Fermi energy with gate voltage considering that the energy gap between two adjacent LLs is $\hbar\omega$.

More quantitatively, according to the Lifshitz-Kosevich model, the temperature dependence of oscillation amplitude follows [45].

$$\Delta R \propto \frac{\lambda(T)}{sinh\ (\lambda(T))} \tag{9}$$

where $\lambda(T) = 2\pi^2 k_B T m^* / \hbar e B$ is the thermal damping factor, k_B stands for Boltzmann constant, $\hbar$ denotes the reduced Plank constant, and m^* is the effective cyclotron mass. **Figure 5a** shows the oscillation component ΔR_{xx} evolves with magnetic field at few different temperatures. The obtained temperature dependence of the oscillation amplitudes accompanied with the fitting result of thermal reduction factor is shown in **Figure 5b** [44]. **Figure 5c** displays the extracted effective cyclotron mass from the fitting result [44]. Similar values of effective cyclotron mass have been reported by different groups [9, 10, 24, 27].

As device quality further improved, Zeeman splitting can be resolved in laboratory-accessible magnetic field [10], and alternative SdH oscillation amplitudes were observed. By reproducing the oscillation component with high-order spin-resolved LK formula

$$\Delta R_{xx} = 2R_0 \sum_{r,\uparrow,\downarrow} \frac{r\lambda(T)}{\sinh(\lambda(T))} \exp\left(-r\frac{\pi}{\omega\tau_{\uparrow,\downarrow}}\right) \cos\left(r\phi_{\uparrow,\downarrow}\right) \tag{10}$$

where ω is the cyclotron frequency, $\lambda(T)$ stands for the thermal factor, $\phi_{\uparrow,\downarrow}$ is the corrected Berry phase taking Zeeman splitting into consideration, and $\tau_{\uparrow,\downarrow}$ is the spin-resolved quantum scattering times. The extracted spin-dependent quantum scattering time at different temperatures and gate voltages are presented in

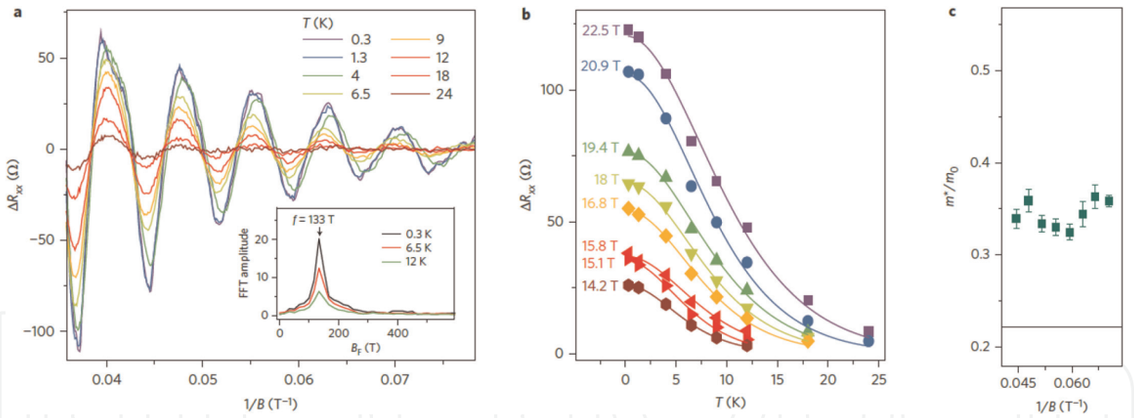

Figure 5.
Effective mass of holes in BP. (a) ΔR_{xx} as a function of 1/B at different temperatures. The inset shows the FFT result at selected temperatures. (b) Evolution of oscillation amplitudes with temperatures at different magnetic fields. The solid lines represent the fitting result of temperature reduction factor. (c) Effective mass of holes obtained from the fitting results shown in panel b. This figure is reproduced with permission from NPG [44].

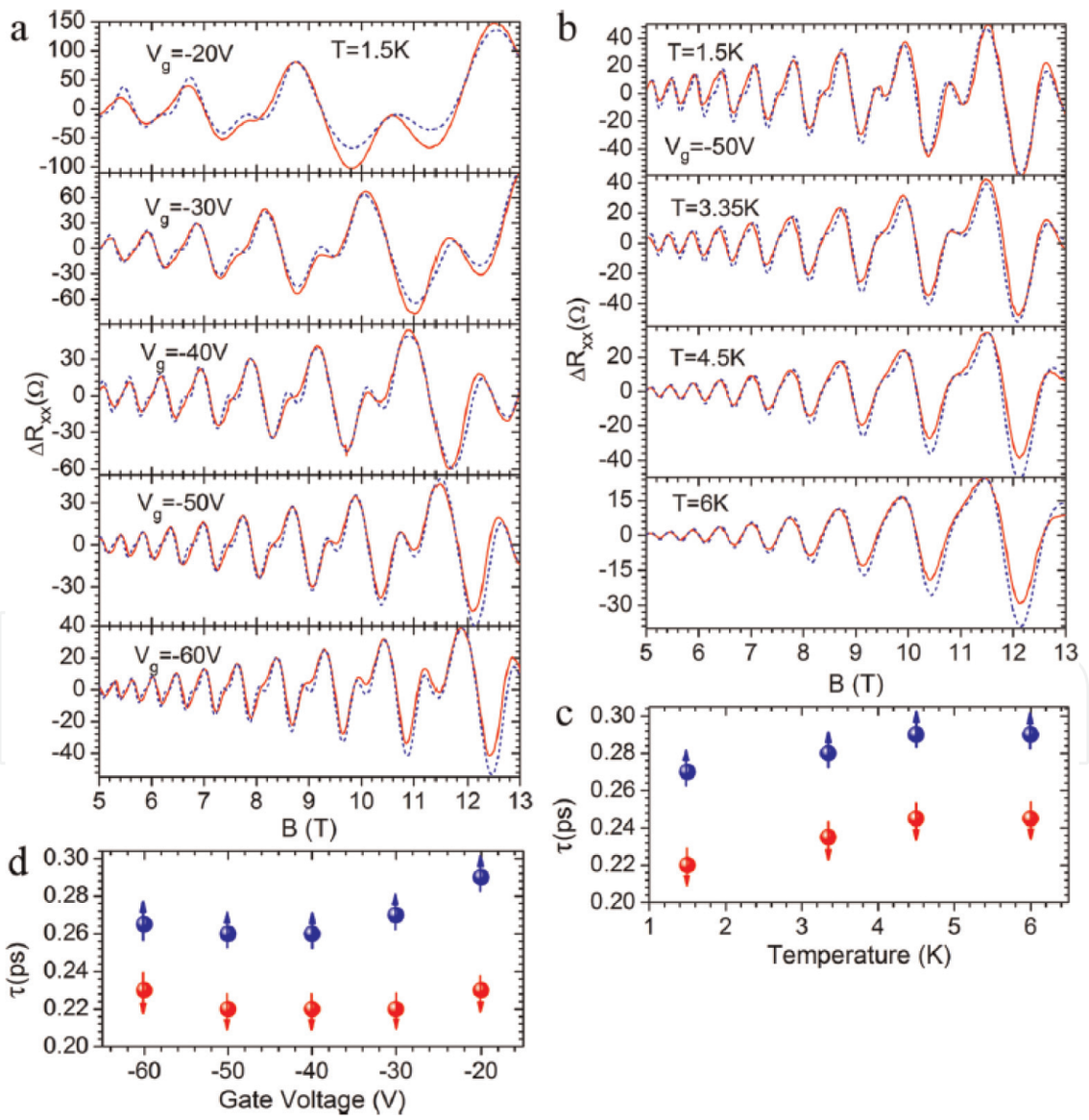

Figure 6.
Spin-selective quantum scattering process (a, b) Oscillation component ΔR_{xx} at selected gate voltages (panel a) and temperatures (panel b). The blue dashed lines present the fitting results of Eq. (10). (c, d) Quantum scattering times for up- and down-spin orientations obtained from the fitting results. This figure is reproduced with permission from ACS [10].

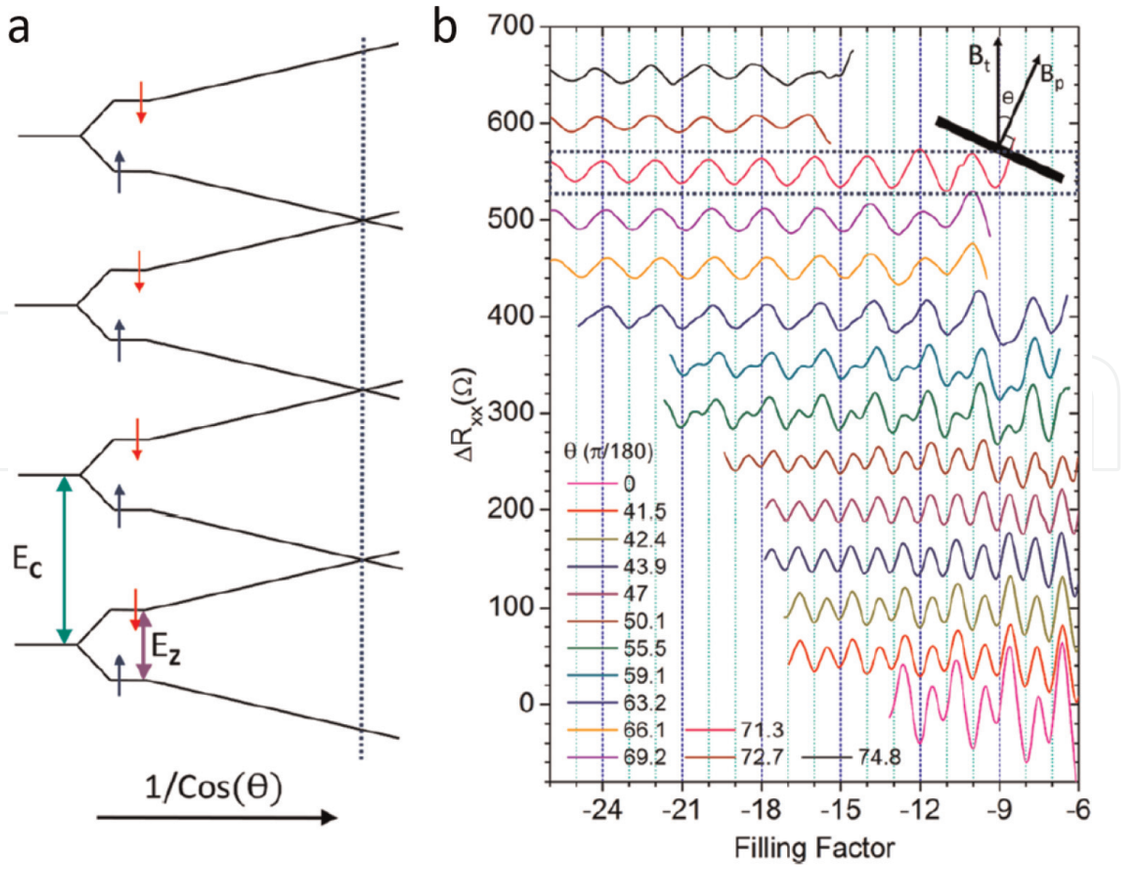

Figure 7.
Coincidence of BP LLs (a) Schematic of spin-resolved LLs evolve with increasing tilting angle at fixed perpendicular magnetic field. The vertical dashed line indicates the coincidence angle θ_c. (b) The evolution of SdH oscillation component with increasing tilting angles. This figure is reproduced with permission from ACS [10].

Figure 6c and **d**, respectively. The charge carriers in BP two-dimensional hole gas (2DHG) show the spin-selective scattering behavior on a phenomenological level. Similar scattering process was also reported in GaAs [46] and ZnO [47] systems. Recently, an analogy called valley-selective scattering process was observed in MoS_2 [48]. The mechanism behind this spin-selective scattering process remains to be further addressed.

The resolvability of Zeeman splitting makes it possible to determine the Landé g-factor of BP electronic systems via the coincidence method taking advantage that the Zeeman energy $E_Z = g\mu_B B_{total}$ depends on the total magnetic field, while the cyclotron energy $E_C = \hbar e B_\perp / m^*$ is determined by the field component $B_\perp$ perpendicular to the 2DHG plane. When the E_Z is a multiple integer of E_C, i.e., $E_Z = iE_C$ (i is an integer number), the spin-resolved LLs overlap. Hence $\chi_s = gm^* = 2i\cos\theta_c$ is valid at coincidence angle θ_c as indicated in **Figure 7a** [10, 49]. **Figure 7b** presents the measurement of coincidence angle, and the extracted spin susceptibility χ_s is $\sim$ 0.64 which leads to a Landé g-factor of $g = 2.47$ [10]. Later on, the same method was applied to electron-doped BP to extract a spin susceptibility of $\sim$ 1.1 and Landé g-factor of $\sim$ 2.8 [29, 50].

Making use of a magnetic field up to 45 T, fractional quantum state at filling factor $\nu = -\frac{4}{3}$ accompanied with quantum feature at -0.56 ± 0.1 was observed in 2018 [51] making BP the second exfoliated van der Waals crystals to exhibit fractional quantum Hall effect after graphene.

When the electronic band of a semiconductor is occupied by induced electrons (e.g., electrons induced by gate voltage), it will screen the electronic field hence prohibiting the wave function of electrons from penetrating the topmost few layers [52–54].

While when the band is empty, it will not screen the electronic field, and the wave function of electrons penetrates all the way to the opposite surface. Based on this screening effect, wide quantum wells have been formed in few-layer BP which can be switched between double layers of charge carriers and single layer of charge carriers [55]. The switch in one single device from double quantum wells and single quantum well has never been realized in other systems. Besides, one can tune the distance between the double layers of charge carriers by selecting *h*BN flakes with different thicknesses. The realization of tunable quantum wells paves the way for using 2D materials as wide quantum wells for investigating phenomena, such as LL hybridization, inter-well Coulomb interactions, or multicomponent quantum Hall ferromagnetism in this highly anisotropic system.

4. Conclusions

In this chapter, we mainly focus on the development of high-quality FET and the electronic transport in quantum limitations based on BP. Although few-layer BP degrades in the atmosphere, encapsulation with BN flakes was proven to be a reliable strategy to realize air-stable devices based on BP. The realization of Ohmic contact through selective etching technique lays the foundation for high-quality devices. Thanks to the rather small electronic bandgaps for few-layer BP flakes, by aligning the work function of contact metals with the band edge of BP, ambipolar-conducting channels were realized in single field effect devices. In devices with high carrier mobility, the scattering rate of charge carriers is low leading to limited broadening of LLs. As a consequence, the LLs become resolvable in laboratory reachable magnetic field at cryogenic temperature. Based on the SdH oscillations and quantum Hall effect, a spin-selective quantum scattering process was established in BP 2DHG. Intrinsic parameters such as effective mass and Landé g-factor were measured. The realization of high-quality air-stable BP devices promises its potential in next-generation electronic applications.

Acknowledgements

The authors acknowledge the financial support from the Research Grants Council of Hong Kong (Project No. FB417- UoM-HKUST and C7036-17 W).

Conflict of interest

The authors declare no conflict of interest.

Author details

Gen Long[1,2†], Xiaolong Chen[1,3†], Shuigang Xu[4†] and Ning Wang[1*]

1 The Hong Kong University of Science and Technology, Hong Kong, China

2 University of Geneva, Geneva, Switzerland

3 Southern University of Science and Technology, Shenzhen, China

4 University of Manchester, Manchester, UK

*Address all correspondence to: phwang@ust.hk

† These authors contributed equally.

References

[1] Xia F, Wang H, Jia Y. Rediscovering black phosphorus as an anisotropic layered material for optoelectronics and electronics. Nature Communications. 2014;**5**:4458

[2] Qiao J, Kong X, Hu Z-X, Yang F, Ji W. High-mobility transport anisotropy and linear dichroism in few-layer black phosphorus. Nature Communications. 2014;**5**:4475

[3] Li L, Yu Y, Ye GJ, Ge Q, Ou X, Wu H, et al. Black phosphorus field-effect transistors. Nature Nanotechnology. 2014;**9**(5):372

[4] Du Y, Liu H, Deng Y, Ye PD. Device perspective for black phosphorus field-effect transistors: Contact resistance, ambipolar behavior, and scaling. ACS Nano. 2014;**8**(10):10035-10042

[5] Sondhi SL, Karlhede A, Kivelson SA, Rezayi EH. Skyrmions and the crossover from the integer to fractional quantum hall effect at small zeeman energies. Physical Review B. 1993;**47**(24):16419

[6] Xiao D, Chang M-C, Niu Q. Berry phase effects on electronic properties. Reviews of Modern Physics. 2010;**82**(3): 1959

[7] Liu H, Neal AT, Zhu Z, Luo Z, Xu X, Tománek D, et al. Phosphorene: An unexplored 2D semiconductor with a high hole mobility. ACS Nano. 2014; **8**(4):4033-4041

[8] Koenig SP, Doganov RA, Schmidt H, Castro Neto AH, Özyilmaz B. Electric field effect in ultrathin black phosphorus. Applied Physics Letters. 2014;**104**(10):103106

[9] Chen X, Yingying W, Zefei W, Han Y, Shuigang X, Wang L, et al. High-quality sandwiched black phosphorus heterostructure and its quantum oscillations. Nature Communications. 2015;**6**:7315

[10] Long G, Maryenko D, Shen J, Shuigang X, Hou J, Zefei W, et al. Achieving ultrahigh carrier mobility in two-dimensional hole gas of black phosphorus. Nano Letters. 2016;**16**(12): 7768-7773

[11] Wang H, Wang X, Xia F, Wang L, Jiang H, Xia Q, et al. Black phosphorus radio-frequency transistors. Nano Letters. 2014;**14**(11):6424-6429

[12] Chen X, Chen C, Levi A, Houben L, Deng B, Yuan S, et al. Large-velocity saturation in thin-film black phosphorus transistors. ACS Nano. 2018;**12**(5): 5003-5010

[13] Castellanos-Gomez A, Vicarelli L, Prada E, Island JO, Narasimha-Acharya KL, Blanter SI, et al. Isolation and characterization of few-layer black phosphorus. 2D Materials. 2014;**1**(2): 025001

[14] Favron A, Gaufrès E, Fossard F, Phaneuf-L'Heureux A-L, Tang NYW, Lévesque PL, et al. Photooxidation and quantum confinement effects in exfoliated black phosphorus. Nature Materials. 2015;**14**(8):826

[15] Du Y, Ouyang C, Shi S, Lei M. Ab initio studies on atomic and electronic structures of black phosphorus. Journal of Applied Physics. 2010;**107**(9):093718

[16] Wood JD, Wells SA, Jariwala D, Chen K-S, Cho EK, Sangwan VK, et al. Effective passivation of exfoliated black phosphorus transistors against ambient degradation. Nano Letters. 2014;**14**(12): 6964-6970

[17] Tayari V, Hemsworth N, Fakih I, Favron A, Gaufrès E, Gervais G, et al. Two-dimensional magnetotransport in a black phosphorus naked quantum well. Nature Communications. 2015;**6**:7702

[18] Avsar A, Vera-Marun IJ, Tan JY, Watanabe K, Taniguchi T, Castro

Neto AH, et al. Air-stable transport in graphene-contacted, fully encapsulated ultrathin black phosphorus-based field-effect transistors. ACS Nano. 2015;**9**(4): 4138-4145

[19] Doganov RA, O'Farrell ECT, Koenig SP, Yeo Y, Ziletti A, Carvalho A, et al. Transport properties of pristine few-layer black phosphorus by van der waals passivation in an inert atmosphere. Nature Communications. 2015;**6**:6647

[20] Cao Y, Mishchenko A, Yu GL, Khestanova E, Rooney AP, Prestat E, et al. Quality heterostructures from two-dimensional crystals unstable in air by their assembly in inert atmosphere. Nano Letters. 2015;**15**(8):4914-4921

[21] Long G, Xu S, Cai X, Wu Z, Han T, Lin J, et al. Gate-tunable strong-weak localization transition in few-layer black phosphorus. Nanotechnology. 2017; **29**(3):5204

[22] Dean CR, Young AF, Meric I, Lee C, Wang L, Sorgenfrei S, et al. Boron nitride substrates for high-quality graphene electronics. Nature Nanotechnology. 2010;**5**(10):722

[23] Wang L, Meric I, Huang PY, Gao Q, Gao Y, Tran H, et al. One-dimensional electrical contact to a two-dimensional material. Science. 2013;**342**(6158): 614-617

[24] Gillgren N, Wickramaratne D, Shi Y, Espiritu T, Yang J, Hu J, et al. Gate tunable quantum oscillations in air-stable and high mobility few-layer phosphorene heterostructures. 2D Materials;**2**(1):011001, 2015

[25] Chen X, Lu X, Deng B, Sinai O, Shao Y, Li C, et al. Widely tunable black phosphorus mid-infrared photodetector. Nature Communications. 2017;**8**(1):1672

[26] Perello DJ, Chae SH, Song S, Lee YH. High-performance n-type black phosphorus transistors with type control via thickness and contact-metal engineering. Nature Communications. 2015;**6**:7809

[27] Long G, Xu S, Shen J, Hou J, Wu Z, Han T, et al. Type-controlled nanodevices based on encapsulated few-layer black phosphorus for quantum transport. 2D Materials. 2016;**3**(3): 031001

[28] Xu S, Wu Z, Lu H, Han Y, Long G, Chen X, et al. Universal low-temperature ohmic contacts for quantum transport in transition metal dichalcogenides. 2D Materials. 2016; **3**(2):021007

[29] Long G, Maryenko D, Pezzini S, Xu S, Wu Z, Han T, et al. Ambipolar quantum transport in few-layer black phosphorus. Physical Review B. 2017; **96**(15):155448

[30] He T, Deng B, Chin ML, Yan X, Jiang H, Han S-J, et al. A dynamically reconfigurable ambipolar black phosphorus memory device. ACS Nano. 2016;**10**(11):10428-10435

[31] Zhu W, Yogeesh MN, Yang S, Aldave SH, Kim J-S, Sonde S, et al. Flexible black phosphorus ambipolar transistors, circuits and AM demodulator. Nano Letters. 2015;**15**(3): 1883-1890

[32] Buscema M, Groenendijk DJ, Steele GA, Van Der Zant HS, Castellanos-Gomez A. Photovoltaic effect in few-layer black phosphorus pn junctions defined by local electrostatic gating. Nature Communications. 2014;**5**: 4651

[33] Wang X, Jones AM, Seyler KL, Tran V, Jia Y, Zhao H, et al. Highly anisotropic and robust excitons in monolayer black phosphorus. Nature Nanotechnology. 2015;**10**(6):517-521

[34] Tran V, Soklaski R, Liang Y, Yang L. Layer-controlled band gap and

anisotropic excitons in few-layer black phosphorus. Physical Review B. 2014; **89**(23):235319

[35] Li L, Kim J, Jin C, Ye GJ, Qiu DY, Felipe H, et al. Direct observation of the layer-dependent electronic structure in phosphorene. Nature Nanotechnology. 2017;**12**(1):21-25

[36] Kim J, Su Baik S, Ryu SH, Sohn Y, Park S, Park B-G, et al. Observation of tunable band gap and anisotropic Dirac semimetal state in black phosphorus. Science. 2015;**349**(6249):723-726

[37] Deng B, Vy T, Xie Y, Jiang H, Li C, Guo Q, et al. Efficient electrical control of thin-film black phosphorus bandgap. Nature Communications. 2017;**8**:14474

[38] Quereda J, San-Jose P, Parente V, Vaquero-Garzon L, Molina-Mendoza AJ, Agraït N, et al. Strong modulation of optical properties in black phosphorus through strain-engineered rippling. Nano Letters. 2016;**16**(5):2931-2937

[39] Zhang Z, Li L, Horng J, Wang NZ, Yang F, Yijun Y, et al. Strain-modulated bandgap and piezo-resistive effect in black phosphorus field-effect transistors. Nano Letters. 2017;**17**(10): 6097-6103

[40] Liu B, Köpf M, Abbas AN, Wang X, Guo Q, Jia Y, et al. Black arsenic–phosphorus: Layered anisotropic infrared semiconductors with highly tunable compositions and properties. Advanced Materials. 2015;**27**(30): 4423-4429

[41] Long M, Gao A, Wang P, Xia H, Ott C, Pan C, et al. Room temperature high-detectivity mid-infrared photodetectors based on black arsenic phosphorus. Science Advances. 2017; **3**(6):e1700589

[42] Yuan S, Shen C, Deng B, Chen X, Guo Q, Ma Y, et al. Air-stable room-temperature mid-infrared photodetectors based on hBN/black arsenic phosphorus/hbn heterostructures. Nano Letters. 2018; **18**(5):3172-3179

[43] Li L, Yang F, Ye GJ, Zhang Z, Zhu Z, Lou W, et al. Quantum hall effect in black phosphorus two-dimensional electron system. Nature Nanotechnology. 2016;**11**(7):593-597

[44] Li L, Ye GJ, Tran V, Fei R, Chen G, Wang H, et al. Quantum oscillations in a two-dimensional electron gas in black phosphorus thin films. Nature Nanotechnology. 2015;**10**(7):608-613

[45] Shoenberg D. Magnetic Oscillations in Metals. Cambridge Monographs on Physics. Cambridge University Press; 1984

[46] Svoboda P, Středa P, Nachtwei G, Jaeger A, Cukr M, Lázníčka M. Current-induced coupling of the edge and bulk channels in GaAs/$Al_xGa_{1-x}As$ heterostructures. Physical Review B. 1992;**45**(15):8763

[47] Maryenko D, Falson J, Bahramy MS, Dmitriev IA, Kozuka Y, Tsukazaki A, et al. Spin-selective electron quantum transport in nonmagnetic MgZnO/ZnO heterostructures. Physical Review Letters. 2015;**115**(19):197601

[48] Lin J, Han T, Piot BA, Wu Z, Xu S, Long G, et al. Determining interaction enhanced valley susceptibility in spin-valley-locked MoS_2. Nano Letters. 2019; **19**(3):1736-1742

[49] Shuigang X, Shen J, Long G, Zefei W, Bao Z-q, Liu C-C, et al. Odd-integer quantum hall states and giant spin susceptibility in p-type few-layer WSe_2. Physical Review Letters. 2017; **118**(6):067702

[50] Yang F, Zhang Z, Zhou Wang N, Jun Ye G, Lou W, Zhou X, et al. Quantum hall effect in electron-doped black phosphorus field-effect

transistors. Nano Letters. 2018;**18**(10): 6611-6616

[51] Yang J, Tran S, Wu J, Che S, Stepanov P, Taniguchi T, et al. Integer and fractional quantum hall effect in ultrahigh quality few-layer black phosphorus transistors. Nano Letters. 2018;**18**(1):229-234

[52] Long G, Xu S, Zhang T, Wu Z, Wong WK, Han T, et al. Charge density wave phase transition on the surface of electrostatically doped multilayer graphene. Applied Physics Letters. 2016; **109**(18):183107

[53] Ye JT, Zhang YJ, Akashi R, Bahramy MS, Arita R, Iwasa Y. Superconducting dome in a gate-tuned band insulator. Science. 2012;**338**(6111): 1193-1196

[54] Lu JM, Zheliuk O, Leermakers I, Yuan NF, Zeitler U, Law KT, et al. Evidence for two-dimensional Ising superconductivity in gated MoS_2. Science. 2015;**350**(6266):1353-1357

[55] Tran S, Yang J, Gillgren N, Espiritu T, Shi Y, Watanabe K, et al. Surface transport and quantum hall effect in ambipolar black phosphorus double quantum wells. Science Advances. 2017;**3**(6):e1603179